Stability Analysis of an Adaptive Notch Filter for RF Noise Suppression

Tim Berenc
Argonne National Laboratory
berenc@aps.anl.gov

Trevor Vannoy
Montana State University
trevor.vannoy@msu.montana.edu

August 25, 2015

Abstract

At the Advanced Photon Source (APS), an adaptive notch filter is being developed to eliminate 60 Hz harmonic noise in the storage ring radio frequency system. Since the adaptive notch filter is in essence a feedback control loop, it is prone to instability. The stability of the adaptive notch filter is analyzed here via the Nyquist stability criterion.

1 Introduction

In particle accelerators, noise in the radio frequency (rf) accelerating voltages causes time jitter and energy fluctuations of the beam. Low-level rf (LLRF) control systems regulate the amplitude and phase of the accelerating voltage, and thus provide noise suppression over the closed-loop bandwidth of the system.

However, a major source of noise in the APS storage ring rf system comes from narrowband noise at 60 Hz. To reduce this 60 Hz harmonic noise, an adaptive notch filter is being developed at the APS [8]. While [8] discussed implementation and demonstration of the adaptive notch filter, a stability analysis is provided here.

The adaptive notch filter is implemented as a feedback control system in which the output of the system is fed back to the input in order to correct for disturbances. A block diagram of a general feedback control system is shown in Fig. 1. Feedback loops are prone to instability (i.e. for a bounded reference input, the controlled output can become unbounded); thus, when implementing a feedback system its stability must be analyzed.

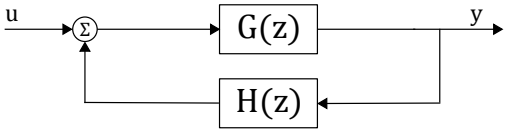

Figure 1: Depiction of a general closed-loop feedback system, with input u and output y.

Various methods exist for analyzing the stability of feedback loops in both the time and frequency domains. In the time domain, for example, system stability can be analyzed by observing the impulse or step response of the system and noting whether or not the response is bounded. In the frequency domain, some of the various methods include root locus, Bode plots, and the Nyquist stability criterion.

Due to its graphical nature, the Nyquist stability criterion is a powerful method, especially for analyzing high order systems and those with time delays. Since the noise suppression system is a very high order system with time delays, the Nyquist stability criterion was chosen to analyze its stability.

2 Review of Nyquist Stability

The Nyquist stability criterion is a graphical method that enables the closed-loop stability of a system to be determined from its open-loop transfer function. Consider the feedback system of Fig. 1 where $G(z)$ and $H(z)$ are represented as rational functions

$$G(z) = \frac{N_g(z)}{D_g(z)} \qquad H(z) = \frac{N_h(z)}{D_h(z)}$$

where $N_g(z)$, $N_h(z)$, $D_g(z)$, and $D_h(z)$ are respectively the numerator and denominator polynomials of $G(z)$ and $H(z)$. The closed-loop transfer function is given as

$$\frac{Y(z)}{U(z)} = \frac{G(z)}{1 + H(z)G(z)} \tag{1}$$

which is expanded as

$$\begin{aligned} \frac{Y(z)}{U(z)} &= \frac{\frac{N_g(z)}{D_g(z)}}{1 + \frac{N_h(z)N_g(z)}{D_h(z)D_g(z)}} \\ &= \frac{N_g(z)}{D_g(z)\left(\frac{D_h(z)D_g(z)+N_h(z)N_g(z)}{D_h(z)D_g(z)}\right)} \end{aligned} \tag{2}$$

In the denominator, $D_g(z)$ will always cancel; hence it will not contribute to any poles of the closed-loop transfer function. Thus the *poles* of the closed-loop transfer function are equivalent to the *zeros* of $1 + H(z)G(z)$. For discrete-time system stability, the *poles* of the closed-loop transfer function must lie within the unit circle in the complex plane. This implies that there can be no *zeros* of $1+H(z)G(z)$ *outside* the unit circle.

2.1 Argument Principle

From complex analysis, the Argument Principle [2, 3, 6] can be used to determine whether there are any *zeros* of $f(z) \equiv 1+H(z)G(z)$ outside the unit circle. The Argument Principle starts with using the following generalized Lucas formula

$$\frac{f'(z)}{f(z)} = \sum_{j=1}^{m} \frac{1}{z-\alpha_j} - \sum_{k=1}^{n} \frac{1}{z-p_k} + \frac{v'(z)}{v(z)} \tag{3}$$

where

$$f(z) = \frac{\prod_{j=1}^{m}(z-\alpha_j)}{\prod_{k=1}^{n}(z-p_k)} \cdot v(z) \tag{4}$$

represents a meromorphic function with a finite number of zeros, α_j, and poles, p_k, in some region Ω. This generalizes $1 + H(z)G(z)$ such that it can include a function $v(z) \neq 0$ which is analytic in Ω. This generalization is especially useful for continuous-time systems for which $v(z)$ can represent the Laplace transform for a time delay which is the transcendental function $e^{-z\tau_d}$. For discrete-time systems, delays equal to an integer number of samples simply add additional poles at the origin.

Next, the following integral is formed

$$\int_\gamma \frac{f'(z)}{f(z)}dz = \sum_{j=1}^{m}\int_\gamma \frac{dz}{z-\alpha_j} - \sum_{k=1}^{n}\int_\gamma \frac{dz}{z-p_k} \tag{5}$$

where γ is a simple closed positively oriented (counter-clockwise) contour on which $f(z)$ is analytic and non-zero. The integrals on the right are solved via complex analysis techniques [3] and are of the form

$$\int_\gamma \frac{dz}{z-z_o} = 2\pi i \tag{6}$$

if z_o lies inside γ. Thus Eq. 5 becomes

$$\frac{1}{2\pi i}\int_\gamma \frac{f'(z)}{f(z)}dz = N_o - N_p \tag{7}$$

where N_o and N_p are respectively the number of zeros and poles of $f(z)$ inside the contour γ as shown in Fig. 2. The geometric nature of the left side of Eq. 7 is revealed by considering [6, Ch. 3, Sec. 10]

$$\frac{1}{2\pi i}\int_\gamma \frac{f'(z)}{f(z)}dz = \frac{1}{2\pi i}\int_\gamma d\,\log f(z) \tag{8}$$

Since $\log f(z) = \log|f(z)| + i\arg\{f(z)\}$ then Eq. 8 becomes

$$\begin{aligned} &\frac{1}{2\pi i}\int_\gamma \frac{f'(z)}{f(z)}dz \\ &= \frac{1}{2\pi i}\int_\gamma d\,\log|f(z)| + \frac{1}{2\pi}\int_\gamma d\arg\{f(z)\} \end{aligned} \tag{9}$$

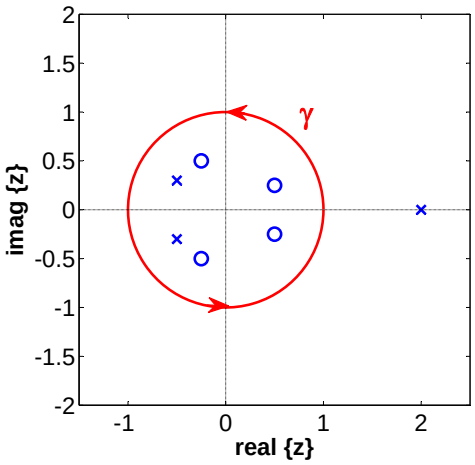

Figure 2: Example contour (γ) integration around poles (x) and zeros (o) in the z-Plane.

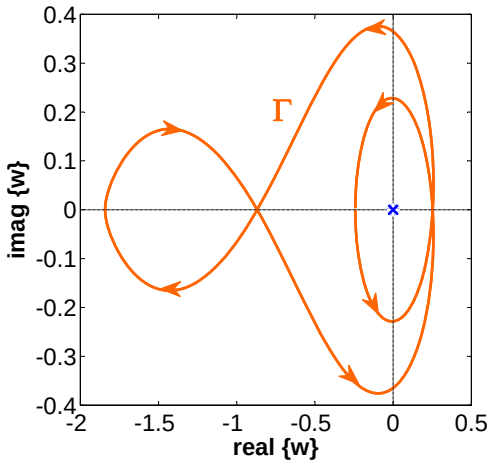

Figure 3: Image contour (Γ) in the w-Plane resulting from the mapping $w = f(\gamma)$.

Because $\log|f(z)|$ is real and single-valued, its integral around the *closed* loop γ reduces to zero. However, because $\arg\{f(z)\}$ is multi-valued, the integral of $d\arg\{f(z)\}$ becomes the net change of $\arg\{f(z)\}$. Using these results, Equation 7 thus becomes

$$\frac{1}{2\pi}\Delta_\gamma \arg\{f(z)\} = N_o - N_p \qquad (10)$$

where $\Delta_\gamma \arg\{f(z)\}$ represents the net change of the *argument* of $f(z)$ evaluated along the contour γ. Hence Eq. 10 is known as the *Argument Principle*.

By defining a new complex variable w such that $w = f(z)$, an image contour $\Gamma = f(\gamma)$ will be traced out in the w-plane as z moves along the contour γ in the z-plane as shown in Figs. 2 and 3. Since γ is closed, so too is Γ. However, Γ need not be simple nor positively oriented.

In the w-plane, $\Delta_\gamma \arg\{f(z)\}$ represents the number of positive (counter-clockwise) encirclements that Γ makes about the origin, denoted as $n_\circlearrowleft\{\Gamma{=}f(z), 0\}$. Thus Eq. 10 can be written as

$$n_\circlearrowleft\{\Gamma{=}f(z), 0\} = N_o - N_p \qquad (11)$$

In the example shown in Figs. 2 and 3, there are 4 zeros and 2 poles inside γ, therefore Γ makes 2 counter-clockwise encirclements about the origin in the w-Plane.

2.2 Nyquist Stability Criterion

As stated earlier, for closed-loop stability of the system in Fig. 1, there should be no *zeros* of $f(z) = 1 + H(z)G(z)$ *outside* the unit circle. An appropriate contour of integration should enclose the entire z-Plane outside the unit circle. Such a contour is shown in Fig. 4 utilizing a cut along the negative real-axis.

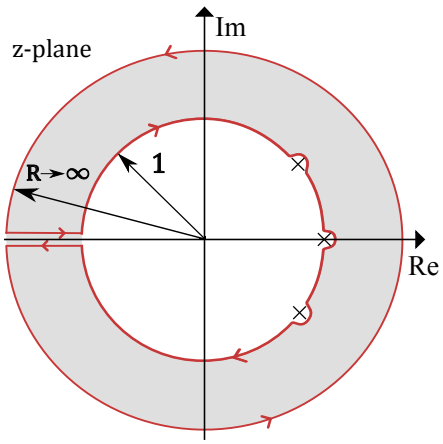

Figure 4: Contour of integration for discrete-time system.

For stability, N_o should be zero and Eq. 11 becomes

$$-n_\circlearrowleft\{\Gamma, 0\} = n_\circlearrowleft\{\Gamma, 0\} = N_p \qquad (12)$$

Because of the negative sign, this states that

for stability the net number of ***clockwise*** encirclements, $n_{\circlearrowleft}$, of the origin by the image curve Γ should be equal to the number of poles inside the positively oriented (*counter-clockwise*) contour of integration γ.

If poles exist along the contour of integration, they can be excluded by modifying the contour with small detours as shown in Fig. 4. The image contour can be formed from a consideration of $f(z)$ being *conformal* along the contour. This *conformal* property means that angles are preserved in the mapping; hence a right-hand turn in the z-plane corresponds to a right-hand turn in the w-plane [2, 7].

Forming the image of the small detours can be avoided by extending the argument principle [6, Ch. 3, Sec. 10]. In the extended principle the zeros and poles on the contour of integration are counted with half of their multiplicity in Eq. 10. While [4, 10] claim an original derivation of this, [6] discussed this much earlier. Since the Nyquist plots to be shown later display the behavior of the detours, the half counting technique will not be utilized.

2.3 $\frac{1}{z}$ Transformation

The contour of integration shown in Fig. 4 is cumbersome since it needs to enclose the entire plane outside the unit circle. Fortunately the conformal mapping $\hat{z} = \frac{1}{z}$ maps the entire plane *outside* the unit circle to *inside* the unit circle [2, Ch. 7].

Forming the composite function [1, Ch. 10]

$$\hat{F}(\hat{z}) = f\left(z = \frac{1}{\hat{z}}\right) \tag{13}$$

the zeros and poles of $f(z)$ inside the unit circle will be taken outside of the unit circle. Similarly, the zeros and poles outside the unit circle will be brought inside the unit circle. Thus looking for *zeros of* $f(z)$ *outside the unit circle* in the z-plane is equivalent to looking for *zeros of* $\hat{F}(\hat{z})$ *inside the unit circle* in the $\hat{z}$-plane.

The contour and region of interest of Fig. 4 transforms to that shown in Fig. 5 in which a

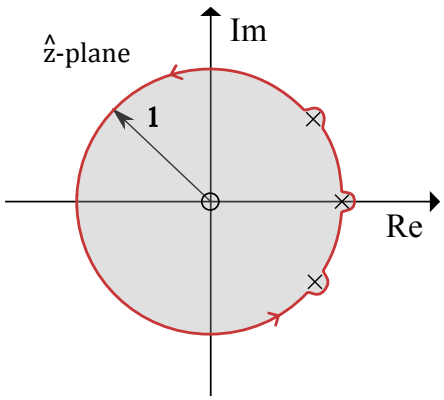

Figure 5: Modified contour of integration for discrete-time system.

counter-clockwise contour along the unit circle is used to satisfy our previous conventions. To use the argument principle, $\hat{F}(\hat{z})$ is evaluated along the unit circle $\hat{z} = e^{i\theta}$ as θ goes from 0 to 2π. Along this contour Eq. 13 gives

$$\hat{F}(e^{i\theta}) = f\left(z = \frac{1}{e^{i\theta}}\right) = f(e^{-i\theta}) \tag{14}$$

This means that evaluating $\hat{F}(\hat{z})$ *counter-clockwise along the unit circle* is equivalent to evaluating $f(z)$ *clockwise along the unit circle* and vice versa. This is apparent in Figs. 4 and 5. However, somewhat magically the cut and outer contour of Fig. 4 *and* forming $\hat{F}(\hat{z})$ are no longer necessary. Thus from Eq. 12, for stability

$$n_{\circlearrowleft}\{\Gamma{=}\hat{F}(\hat{z}{=}\circlearrowleft), 0\} = n_{\circlearrowleft}\{\Gamma{=}f(z{=}\circlearrowleft), 0\} = N_p \tag{15}$$

where $\hat{z}{=}\circlearrowleft$ and $z{=}\circlearrowleft$ are respectively used to represent the counter-clockwise and clockwise unit circle contours in the $\hat{z}$-plane and the z-plane, and N_p represents the number of poles of $f(z)$ outside the unit circle.

2.3.1 Subtlety of the Transformation

There is a subtlety to the above approach which is worth mentioning since we have not found it in the literature. The mapping $z = \frac{1}{\hat{z}}$ also brings zeros and poles of $f(z)$ at *infinity* to the origin of the $\hat{z}$-plane, which is obviously inside the unit circle. For example a zero at α_j will

transform from $(z-\alpha_j)$ to $\left(\frac{1}{\hat{z}}-\alpha_j\right)$ which becomes $\frac{(1-a\hat{z})}{\hat{z}}$. Thus the zero at α_j is indeed transformed into a zero at $\frac{1}{\alpha_j}$. However, the corresponding pole at *infinity* of the expression $(z-\alpha_j)$ is transformed into a pole at the origin. Similarly, a pole at p_k will transform into a pole at $\frac{1}{p_k}$ and the associated zero at *infinity* of the expression $\frac{1}{(z-p_k)}$ will be transformed into a zero at the origin.

As Eq. 15 implies, one gets the same number of encirclements from $\Gamma=\hat{F}(\hat{z}=\circlearrowleft)$ as that from $\Gamma=f(z=\circlearrowleft)$. Although a zero inside the unit circle may be transformed into a zero outside the unit circle, the integral is the same because the zero at *infinity* was pulled to the origin. What works is that the transfer function $f(z)=1+H(z)G(z)$ will have the same number of poles as there are zeros unless there is positive feedback with a biproper (same number of zeros and poles) $H(z)G(z)$ for which the highest order term in the numerator could cancel when performing the addition $1+H(z)G(z)$. In that case, the number of zeros of $f(z)$ will be less than the number of poles and the system is unstable and even unphysical (the closed-loop system would then have more zeros than poles). The stability condition above will properly catch this case. In most cases the number of zeros and poles will be the same, thus the zeros and poles at *infinity* that are brought to the origin will cancel as well as their contributions to the integral. In either case, one can safely determine whether there were indeed zeros α_j of $f(z)$ outside the unit circle.

2.4 Nyquist Plots

A Nyquist plot is a plot of the image contour Γ obtained from the mapping of $f(z)$ along γ. Engineering typically uses a *counter-clockwise* contour along the unit circle, $z=\circlearrowleft$, when constructing the Nyquist plot for discrete-time systems. There is nothing wrong with this. Equation 15 is simply rewritten as

$$n_{\circlearrowleft}\{\Gamma=f(z=\circlearrowleft),0\}=N_p \tag{16}$$

where the net number of *counter-clockwise* encirclements made by Γ are counted.

Earlier $f(z)$ was defined such that

$$f(z)=1+L(z) \tag{17}$$

where $L(z)=H(z)G(z)$ is the total loop transfer function. Equation 17 implies that $f(z)$ has the same poles as $L(z)$ and also that $L(z)=-1$ when $f(z)=0$. A plot of $f(z)$ is simply a right shift of $L(z)$ by 1 unit along the real axis. Instead of making this right shift, a Nyquist plot shows the image contour $\Gamma=L(z=\circlearrowleft)$. Encirclements of the origin by $\Gamma=f(z=\circlearrowleft)$ thus become equivalent to encirclements of the point -1 by $\Gamma=L(z=\circlearrowleft)$. Equation 16 then becomes

$$\boldsymbol{n_{\circlearrowleft}\{\Gamma=L(z=\circlearrowleft),-1\}=N_p} \tag{18}$$

For stability, the number of *counter-clockwise* encirclements of the point -1 by the Nyquist plot of $L(z=\circlearrowleft)$ must equal the number of poles of $L(z)$ which lie outside the unit circle.

3 The Adaptive Notch Filter

The general case of an adaptive noise canceller is shown in Fig. 6. Noise n pollutes a desired signal d. A noise reference, x, which is correlated to n is fed into an adaptive filter $A(z)$. The output of $A(z)$ is combined with the noisy signal, $s=d+n$, to cancel the noise. The filter is adapted in a way which minimizes the output, ϵ, in the least mean squares sense. [9].

If the noise source has a broad frequency spectrum, many filter coefficients are needed to make the filter output match the noise. However, if the noise is narrowband or contains only a single line harmonic, the filter can be implemented as an adaptive notch filter with only two coefficients, w_I and w_Q, as shown in Fig. 7. The feedback loop automatically finds an in-phase and quadrature component, y_I and y_Q respectively,

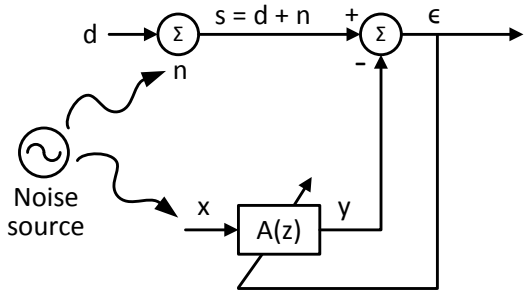

Figure 6: Depiction of a general adaptive noise canceller

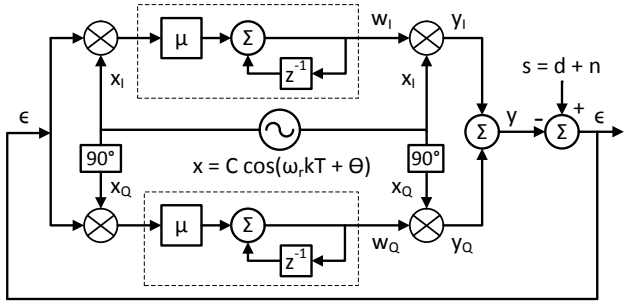

Figure 7: Block diagram of the two-weight adaptive notch filter

of the noise reference which will cancel the noise at the output.

The open-loop transfer function, $H(z)$, from ϵ to y is [8]

$$H(z) = \mu C^2 \frac{z\left(z - \cos(\omega_r T)\right)}{\left(ze^{-i\omega_r T} - 1\right)\left(ze^{i\omega_r T} - 1\right)} \qquad (19)$$

where $i = \sqrt{-1}$, ω_r is the noise reference frequency, T is the sample time, z is the z-transform variable, C is the magnitude of the noise reference, and μ is a loop gain parameter.

The closed-loop transfer function, from s to ϵ, is given by

$$\frac{E(z)}{S(z)} = \frac{1}{1 + H(z)}$$

$$= \frac{\left(ze^{-i\omega_r T} - 1\right)\left(ze^{i\omega_r T} - 1\right)}{(1 + \mu C^2)z^2 - \cos(\omega_r T)(2 + \mu C^2)z + 1} \; . \qquad (20)$$

Equation 20 describes the desired behavior of the adaptive notch filter. The transfer function has a zero at the noise reference frequency ω_r, thus eliminating noise at that frequency. The bandwidth of the filter is controlled by the noise reference amplitude C and the gain μ.

3.1 System Implementation Details

The adaptive notch filter shown in Fig. 7 is a simplified version of its actual implementation. The prototype system at the APS uses many more digital filters and some external analog components. A detailed block diagram of the system is shown in Fig. 8.

Analog low-pass filters (LPF) are used on the input signals (reference x and error ϵ) to prevent aliasing before being digitized by the analog-to-digital converters (ADC). The signals are sampled at 100kSamples/sec (kS/sec) and then decimated to 10kS/sec. A 57^{th} order LPF is used prior to the decimation to prevent aliasing. The digital filtering and decimation relax the requirements of the analog input filters.

The decimated reference signal then goes through a Hilbert transform filter that generates two output signals which are in quadrature with each other. The Hilbert transform filter is composed of two separate low-pass type filters one for each the in-phase and quadrature component. The coefficients are determined from a 60^{th} order LPF prototype according to the technique of [5].

Since the outputs of the Hilbert filter are still broadband, both components go through a 400^{th} order bandpass filter (BPF) before becoming the in-phase and quadrature reference signals for the adaptive filter. This provides extreme selectivity of the 60Hz harmonic component of interest.

Ideally, the quadrature outputs from the Hilbert filter have identical amplitudes; however, in practice they do not. Thus the scalings g_I and g_Q in Fig. 8 are used to represent an amplitude imbalance. The imbalance can cause sum and difference frequencies generated in the down/up conversion process (represented as the multipliers) to not cancel in the final output. This can generate unwanted spectral content in the output signal. In addition to representing the amplitude imbalance from the Hilbert filter, g_I and g_Q also serve to represent various gain terms that ac-

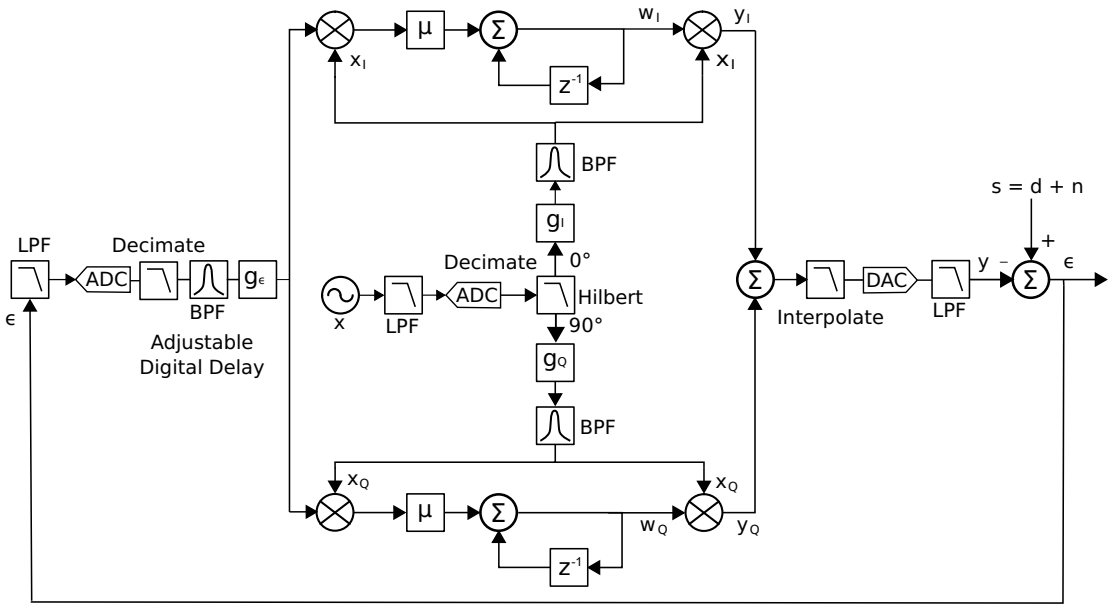

Figure 8: Detailed block diagram of the adaptive notch filter.

count for external analog circuitry and the band-pass filters.

The sampled and decimated error signal also goes through the 400^{th} order BPF to select the 60Hz harmonic of interest. The scaling represented by g_ϵ in Fig. 8 summarizes various gain terms: gain from the band-pass filter, gain from the reconstruction and decimation filter, gain from moving the binary point in the signal's fixed-point representation, and gain from external analog circuitry.

The error signal also goes through an adjustable digital delay with coarse adjustments in 10kS/sec clock ticks. This delay provides a means to optimize the loop phase and hence system stability.

The error signal is then down-converted by both the in-phase and quadrature reference signals. Each of the down-converted signals goes through an integrator with gain μ before being up-converted and summed together. This digital sum then goes through the same 57^{th} order LPF used for the decimation process before being interpolated back to 100kS/sec. Finally the analog output is generated by the DAC followed with a reconstruction analog LPF.

Each component and signal path of the system was meticulously measured and modeled using Matlab and Mathematica. The system is represented by the following open-loop transfer function $\mathcal{H}(z)$

$$\mathcal{H}(z) = z^{-\tau} \frac{g_{total}\, z\,(z - \cos(\omega_r T))}{(ze^{-i\omega_r T} - 1)\,(ze^{i\omega_r T} - 1)} \mathcal{B}(z)\mathcal{L}(z) \tag{21}$$

where

$$g_{total} = \frac{\mu C^2}{2}\left(g_I^2 + g_Q^2\right) g_\epsilon$$

$z^{-\tau}$ represents a time delay τ, and $\mathcal{B}(z)$ and $\mathcal{L}(z)$ are the transfer functions for the BPFs and LPFs respectively.

3.2 Stability Analysis Results

The adaptive filter $\mathcal{H}(z)$ has poles on the unit circle but none outside the unit circle. Thus a detoured contour such as that shown in Fig. 5 is appropriate. For stability of the system, equation 18 applies as follows

$$n_{\circlearrowleft}\{\Gamma{=}\mathcal{H}(z = \circlearrowleft), -1\} = 0 \tag{22}$$

In other words, there should be no *counter-clockwise* encirclements of the point -1 made by the Nyquist plot of $\mathcal{H}(z)$.

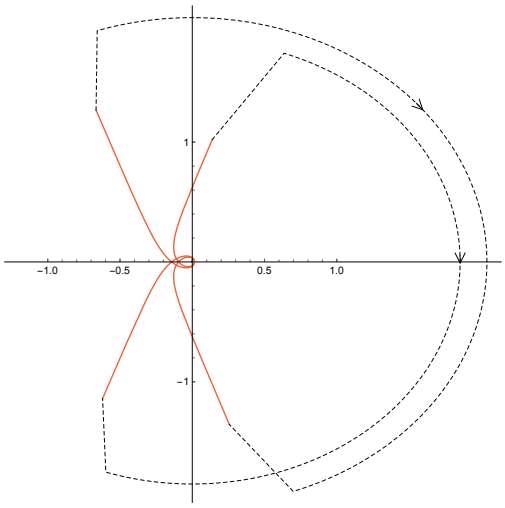

Figure 9: Nyquist plot for $\mu = 1$, a 33 sample delay, and $C = 0.05$ V.

Due to the poles on the unit circle, the open-loop response cannot be directly measured. Instead, the closed-loop response is measured and compared to the theoretical closed-loop response, $1/(1 + \mathcal{H}(z))$. A Stanford Research Systems SR-785 dynamic signal analyzer was used to make the measurements.

For $\mu = 1$, a 33 sample delay, and $C = 0.05$ V, the Nyquist plot in Fig. 9 shows that the system should be stable; the closed-loop response in Fig. 10 confirmed this. While the experimental response in Fig. 10 does resemble the theoretical response, it exhibits noise near 60 Hz. This noise was found to be due to the amplitude imbalance from the Hilbert filter. As the frequency approaches 60 Hz, the uncancelled upper or lower sideband gets increasingly close to 60 Hz and makes its way into the bandwidth of the analyzer's detection filter.

To correct the amplitude mismatch, a multiplier was added to the in-phase component. With the multiplier properly adjusted, the noise was nearly eliminated as seen in Fig. 11. In addition to eliminating the noise, the multiplier slightly increased the open-loop gain.

For a higher system gain of $\mu = 0.8$, a 22 sample coarse delay, and a reference signal amplitude $C = 0.1$ V, the theoretical and measured closed-loop responses are shown in Fig. 12. The predicted magnitude response peaks more sharply than the measured response. The predicted phase also does not match the measured phase near the peak in the magnitude response. By adding 3 samples of group delay to the model, the theoretical and experimental responses matched each other extremely well as seen in Fig. 13. This finding suggests that there are approximately 3 samples worth of group delay in the system that are not accounted for in the model.

With confidence in the theoretical model having been established, it was possible to predict when the system should go unstable. As an example, for $\mu = 1.2$, a 25 sample delay, and $C = 0.1$ V, the Nyquist plot in Fig. 14 shows that the system should be unstable. We experimentally observed that the system does indeed become unstable for these settings as evidenced in Fig. 15.

4 Conclusion and Future Work

We provided a thorough review of the Nyquist stability criterion for discrete-time systems, creating a fairly comprehensive review derived from multiple references. While the criterion for continuous-time systems is discussed extensively in the literature, that for discrete-time systems is rather scant. We also presented a discussion about the $\frac{1}{z}$ transformation pulling zeros and poles at *infinity* to the origin; something which we have not seen addressed in the literature.

An extensive model for the adaptive notch filter was meticulously developed. After correcting for a suspected 3 sample delay error, the model can very accurately predict the closed-loop response. Furthermore, the closed-loop response measurements with the dynamic signal analyzer can take almost half an hour while the theoretical calculation takes mere seconds.

There are some areas that can use additional work. The source of the 3 sample delay error should be investigated. The amplitude imbalance of the Hilbert filter should also be more fully explored. Finally, the analysis presented here was for the 60Hz channel of the noise sup-

pression system. The system consists of additional channels for other 60Hz harmonics. Similar analyses of these additional channels should be performed. Although in theory these should all be modeled in parallel, they should be able to be analyzed independently due to the isolation offered from the highly selective band-pass filters in each channel.

5 References

References

[1] A.S. Willsky A.V. Oppenheim, *Signals and systems*, 2nd ed., Prentice Hall, 1996.

[2] A.D. Snider E.B. Saff, *Complex analysis for mathematics, science, and engineering*, 2nd ed., Prentice Hall, New Jersey, 1993.

[3] C. W. Gray, *Complex variables*, The Control Handbook, 2nd Edition (W. S. Levine, ed.), CRC Press, 2011.

[4] H.M. Lai K.S. Yeung, *A reformulation of Nyquist criterion for discrete systems*, IEEE Transactions on Education **31** (1988), no. 1.

[5] R. Lyons, *Understanding digital signal processing*, 2nd ed., Prentice Hall, 2004.

[6] Zeev Nehari, *Conformal mapping*, Dover, New York, 1975, (Original work published 1952).

[7] C. E. Rohrs, *The nyquist stability test*, The Control Handbook, 2nd Edition (W. S. Levine, ed.), CRC Press, 2011.

[8] K. Cook T. Berenc, *RF noise suppression for the APS storage ring*, Tech. Report RF-TN-2014-004, APS/ASD/RF, 2014, `http://www.illinoisacceleratorinstitute.org/2014%20Program/student_papers/Kevin_Cook.pdf`.

[9] B. Widrow, *Adaptive noise cancelling: Principles and applications*, Proceedings of the IEEE **63** (1975), no. 12, 1692–1716.

[10] K.S. Yeung, *A reformulation of Nyquist's criterion*, IEEE Transactions on Education **E-28** (1985), no. 1.

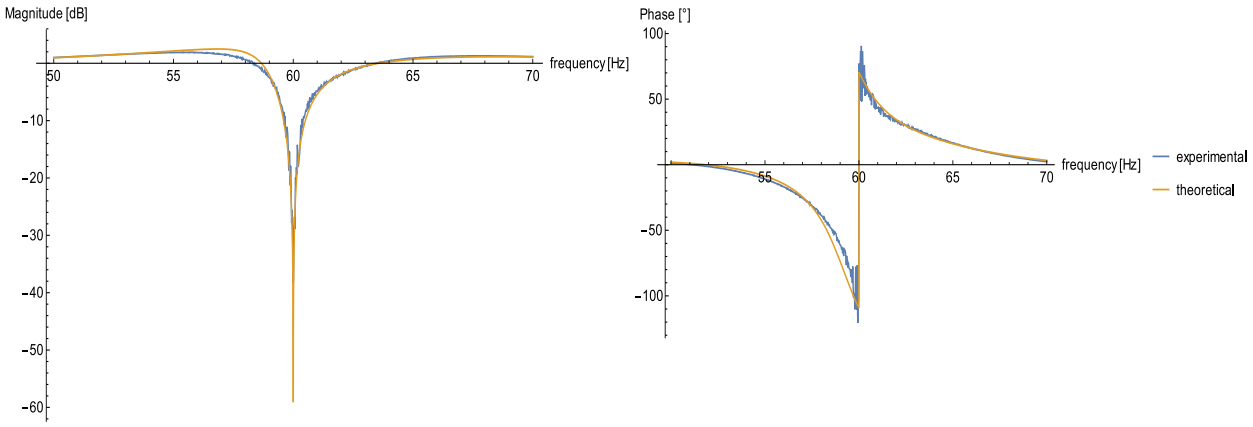

Figure 10: Closed-loop responses for $\mu = 1$, a 33 sample delay, and $C = 0.05$ V.

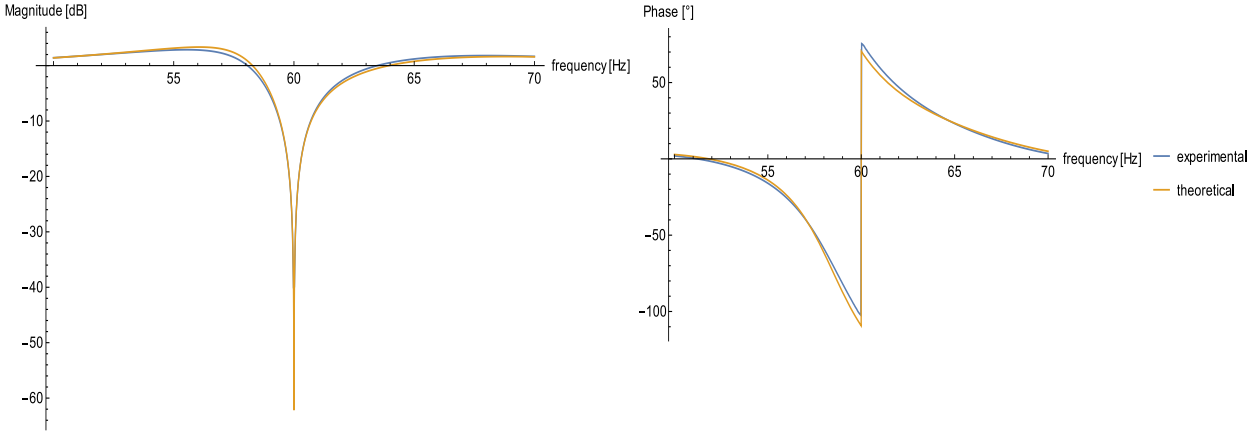

Figure 11: Closed-loop responses for $\mu = 1$, a 33 sample delay, and $C = 0.05$ V with the improved Hilbert filter.

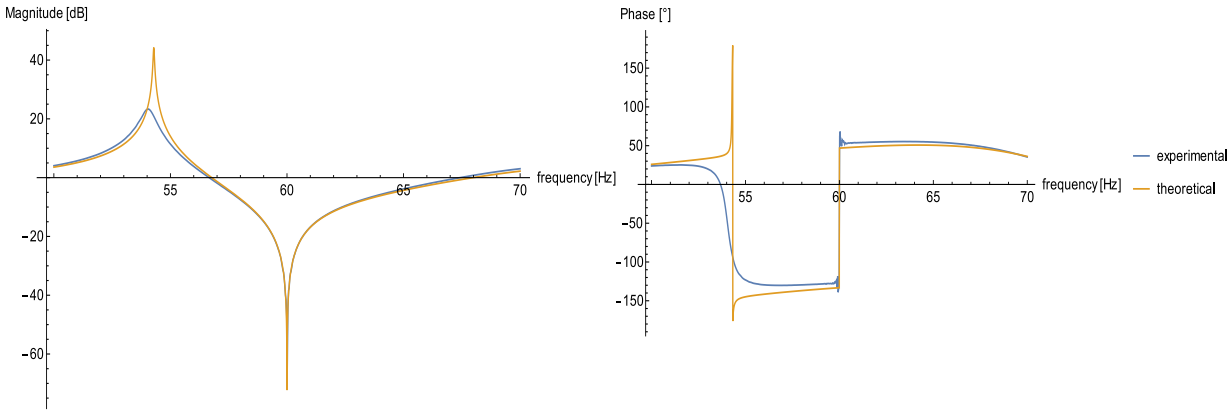

Figure 12: Closed-loop responses *without* corrected group delay for $\mu = 0.8$, a 22 sample delay, and $C = 0.1$ V.

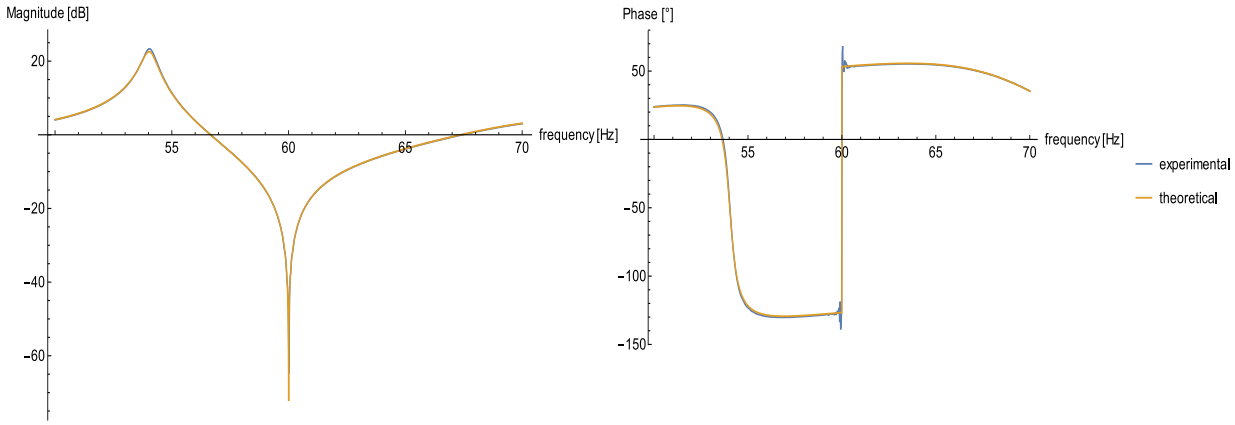

Figure 13: Closed-loop responses *with* corrected group delay for $\mu = 0.8$, a 22 sample delay, and $C = 0.1$ V.

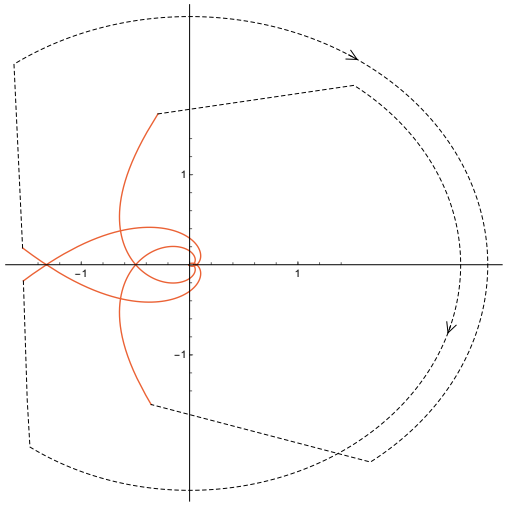

Figure 14: Nyquist plot predicting instability for $\mu = 1.2$, a 25 sample delay, and $C = 0.1$ V.

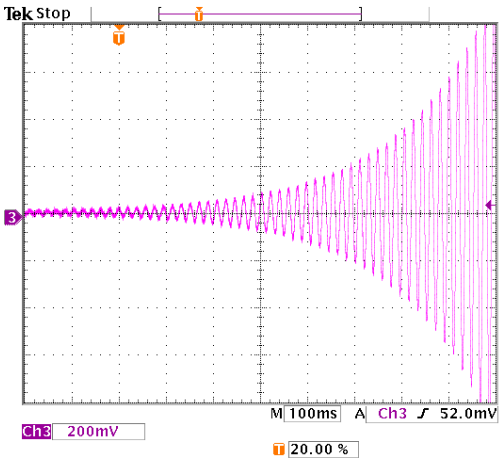

Figure 15: Oscilloscope screenshot of the system going unstable